


Chitosan-based spray-dried solid dispersions of apigenin in a 3D printable drug delivery system

Amer S. Alali¹ | Mohammed Muqtader Ahmed¹ | Farhat Fatima¹ |
Md. Khalid Anwer¹ | Mutasim Ibnauf¹ | M. Ali Aboudzadeh² 

¹Department of Pharmaceutics, College of Pharmacy, Prince Sattam Bin Abdulaziz University, Al-Kharj, Saudi Arabia

²POLYMAT and Department of Polymers and Advanced Materials: Physics, Chemistry and Technology, Faculty of Chemistry, University of the Basque Country UPV/EHU, Donostia-San Sebastián, Spain

Correspondence

Mohammed Muqtader Ahmed,
Department of Pharmaceutics, College of Pharmacy, Prince Sattam Bin Abdulaziz University, P.O. Box 173, Al-Kharj 11942, Saudi Arabia.
Email: mo.ahmed@psau.edu.sa

M. Ali Aboudzadeh, POLYMAT and Department of Polymers and Advanced Materials: Physics, Chemistry and Technology, Faculty of Chemistry, University of the Basque Country UPV/EHU, Paseo Manuel de Lardizabal 3, 20018, Donostia-San Sebastián, Spain.
Email: mohammadali.aboudzadeh@ehu.eus

Funding information

Prince Sattam bin Abdulaziz University, Grant/Award Number: PSAU/2023/03/25933

Abstract

This study aims to develop chitosan-based apigenin (AGN) spray-dried solid dispersions (SDSDs) within a 3D pill. AGN SDSDs were prepared using 1:1 (AC1), 1:1.5 (AC2), and 1:2 (AC3) apigenin/chitosan weight ratios. The results of the process yield were found to be (87.5%, 94.2%, and 95.86%) and of drug assay were obtained as ($95.2 \pm 1.34\%$), ($99.5 \pm 0.85\%$) and ($97.6 \pm 2.42\%$) for AC1, AC2 and AC3, respectively. FTIR revealed compatibility between chitosan and apigenin. DSC and XRD revealed an amorphous state of developed solid dispersions. In contrast, SEM images reflected irregular-block and near-spherical-shape elongated particles in the selected AC2. The antimicrobial examination reflected that AC2 was more effective against Gram-positive, –negative, and fungal strains. AC2 SDSDs had more antioxidant property compared to pure AGN. The anti-proliferative activity against A549 lung cancer cell lines showed a better anticancer activity by AC2 SDSDs. Selected AC2 SDSD was filled in a 3D shell pill and was further characterized in terms of stability. The product had a sustained release and similar release profiles after 3 months of storage. The findings suggest that AC2 SDSDs could be a promising candidate for further development as a 3D-printed drug delivery system for treating multiple disease conditions.

KEYWORDS

biomaterials, differential scanning calorimetry, drug delivery systems, polysaccharides

1 | INTRODUCTION

Chitosan (CTN) is a biocompatible, biodegradable material derived from chitin. It is nontoxic and mucoadhesive, making it ideal for adhering to mucosal surfaces and enhancing drug delivery.^{1,2} CTN has a variety of potential applications in industries such as pharmaceuticals,

biotechnology, agriculture, and food.³ CTN can be extracted from shrimp, crab, and lobster shells through deproteinization, demineralization, and deacetylation, or from other sources than seafood waste, such as fungi, insects, and algae, including *Aspergillus niger* and beetles.^{4,5} Commercially, CTN is available in various forms like powder and flakes. Its molecular weight, influenced

This is an open access article under the terms of the [Creative Commons Attribution-NonCommercial](https://creativecommons.org/licenses/by-nc/4.0/) License, which permits use, distribution and reproduction in any medium, provided the original work is properly cited and is not used for commercial purposes.

© 2024 The Author(s). *Journal of Applied Polymer Science* published by Wiley Periodicals LLC.

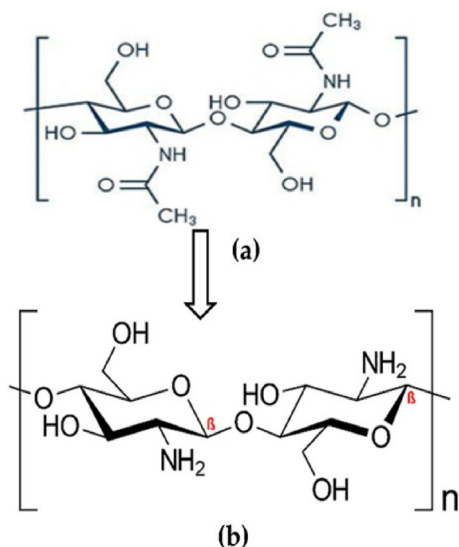


FIGURE 1 Framework of (a) chitin and (b) chitosan. β-(1 → 4)-linked **D-glucosamine** (deacetylated unit) and **N-acetyl-D-glucosamine** (acetylated unit). [Color figure can be viewed at wileyonlinelibrary.com]

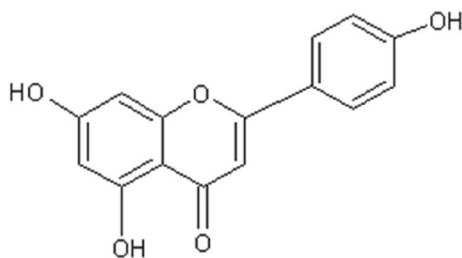


FIGURE 2 Chemical structure of apigenin.

by the chitin source and degree of deacetylation, affects its solubility and viscosity. CTN chitosan exhibits low solubility in water at neutral pH, but adding acetic acid enhances solubility due to its amino groups.⁴ (Figure 1).

CTN is used in drug delivery for its mucoadhesion, permeation enhancement, and controlled release properties. It is commonly used in nanoparticles, microparticles, hydrogels, and films to deliver therapeutic agents like anticancer drugs, antibiotics, and anti-inflammatory agents.⁶ Microencapsulation prepared by CTN has been exploited to deliver proteins, peptides, and vaccines.⁷ Muqtader et al. reported chitosan-based gels for wound-healing activity.⁸ Studies also reflect the transdermal and buccal films loaded with timolol and nicotine.⁹ The cation in CTN enhances the adherence of drug delivery systems to mucosal surfaces (ocular, nasal, gastrointestinal, respiratory, rectal, vaginal), improving drug absorption, bioavailability, and residence time at the action site.¹⁰ CTN can also improve drug permeation at the blood-brain barrier (BBB) due to its ability to open tight

junctions between cells.¹¹ Brigatinib loaded in PLGA nanoparticles coated with CTN was explored for treating non-small cell lung cancer.¹² CTN-coated bupirone-loaded nanostructured lipid carriers for intranasal delivery used for a nose to brain delivery.¹³ In vivo, pharmacokinetic Studies of CTN-coated PLGA-based NPs have shown the enhanced bioavailability of olaparib.¹⁴

Apigenin (AGN, structure shown in Figure 2) is a flavonoid found in plants such as parsley, chamomile, and celery. AGN has multiple health benefits that some of them has been reported herein.¹⁵ AGN has sequestering properties that neutralize free radicals, protecting cells from damage due to cancer, aging, and inflammation. AGN reduces inflammation by inhibiting cyclooxygenases (COX) and lipoxygenases (LOX) enzymes, which produce inflammatory molecules, and blocking nuclear factor-kappa B (NF-κB) activation. This decreases chronic inflammation linked to heart disease, diabetes, and cancer.^{16,17} AGN acts as an anticancer agent by regulating signaling pathways involved in cell cycle progression, angiogenesis, and metastasis, inhibiting the growth of various cancer cells and reducing cancer risk. AGN-induced apoptosis helps prevent cancer spread.¹⁸ AGN has anxiolytic properties by acting on gamma-aminobutyric acid (GABA) in the brain and modulating serotonin and dopamine neurotransmitters, aiding in anxiety regulation and treatment of Alzheimer's and Parkinson's diseases.¹⁹ AGN also disrupts bacterial enzyme activity involved in metabolism and DNA replication, enhancing its antimicrobial effects and making it a potentially valuable natural remedy for infections.²⁰ As AGN arrests reactive oxygen species (ROS) in the body, which can help protect against damage to blood vessels and reduce the risk of atherosclerosis.²¹ Additionally, AGN prevents blood clots and improves endothelial function, reducing blood pressure, improving lipid profiles, and lowering heart disease risk.^{22,23} AGN improves insulin sensitivity and glucose uptake, inhibits carbohydrate metabolism enzymes, and may serve as a valuable natural remedy for diabetes and related complications.²⁴

AGN is a yellow crystalline powder with a bitter taste and it is sparingly soluble in water but not in organic solvents such as dichloromethane, chloroform, ethanol, methanol, and dimethyl sulfoxide (DMSO).^{25,26} Studies show that AGN combined with doxorubicin has better anticancer effects compared to doxorubicin alone.²⁷ Another study showed that AGN bound to mucous membranes in the body and improved drug absorption.²⁸ Additionally, AGN nanoparticles of curcumin showed an improved solubility and bioavailability of curcumin, leading to enhanced therapeutic effects.²⁹

Solid dispersion (SD) systems have shown promising results in improving the bioavailability of poorly soluble

drugs, in which the drug can exist in various forms, including crystalline, amorphous, or both. An amorphous form of the drug has a relatively better dissolution rate and therapeutic effects with reduced doses.^{30–32} Technologies employed in preparing SDs are solvent evaporation, freeze-drying, hot-melt extrusion, and spray drying.³³ Spray-drying technology is commonly used for preparing SDs in the pharmaceutical industry and lab setups and was chosen in this study as it offers low operating costs and is an energy-efficient technology, making it a cost-effective choice for large-scale production. Additionally, the fast processing times and high encapsulation efficiency of this technique help maintaining the stability and effectiveness of the active ingredient during scale-up.³⁴ The process involves dissolving the drug (AGN) and a polymer (CTN) in a solution, atomizing it into an air chamber supplied with hot air, and producing a powder of drug–polymer particles known as spray-dried solid dispersions (SDSDs).³⁵ MM Ahmed et al. reported the improved dissolution and aphrodisiac activity of sildenafil and tadalafil SDSDs using glycyrrhizin.^{31,36,37} A spray-dried amorphous solid dispersion of diosmin in Soluplus was prepared by MK Anwer et al. and reported to show improved hepato-renal protective and antioxidant properties.³⁸

Three-dimensional (3D) printing is a promising technology in the pharmaceutical industries and drug development, especially for personalized medicines which offers the advantage of precise customization, allowing for the creation of complex geometries and optimized drug formulations tailored to individual needs. It enhances efficiency by minimizing waste and enabling rapid prototyping of new soft capsules' designs. However, it comes with high costs, require advanced technical expertise, face challenges in scaling up production, and may not be compatible with all drug formulation. Also, the printed capsules may have limited flexibility once formulated due to the potentially shorter shelf lives depending on the stability of the encapsulated compounds.^{39,40}

To the best of our knowledge, the investigation of spray-dried solid dispersion of apigenin with chitosan has not yet been reported. The study aimed to develop and characterize chitosan-based spray-dried solid dispersions (SDSDs) of apigenin. First, we prepared the chitosan-based SDSDs of apigenin by optimizing the process parameters, such as the chitosan concentration, the ratio of apigenin to chitosan, and the spray-drying conditions. Characterization techniques included Fourier transform infrared spectroscopy (FTIR), differential scanning calorimetry (DSC), X-ray diffraction (XRD), and scanning electron microscopy (SEM). Finally, we fabricated a three-dimensional (3D) printer using polyvinyl alcohol

(PVA) filament (used as support material) filled with AGN-CTN SDSDs and assessed their release behavior and content analysis.

2 | RESULTS AND DISCUSSION

2.1 | Process yield-percentage

The calculated yield of AC1, AC2, and AC3 was found to be 87.5%, 94.2%, and 95.86%, respectively. The unit operations of weighing, mixing, agitations, material adherence to the glassware, and pipetting used in the spray-drying operation could be the factors for the loss of yield. Notably, the experimental results showed a higher yield for AC3 compared to AC1 and AC2 SDSDs. This suggests that the formulation or process conditions associated with AC3 were more promising, but to optimize the batch on large scale, a further characterization would be considered.

2.2 | Drug assay

The drug assay of three batches revealed that the amount of active pharmaceutical ingredient (AGN) in the SDSDs was within pharmacopoeial limits.⁴¹ The percentage of AGN in AC1, AC2, and AC3 were found to be $95.2 \pm 1.34\%$, $99.5 \pm 0.85\%$, and $97.6 \pm 2.42\%$, respectively. As per the USP (United States Pharmacopoeia) monograph, a standardized document, the drug content limit should be between 98.0% to 102.0%, a legally acceptable guideline for the quality control of drug products. These results confirmed that only batches AC2 and AC3 were acceptable for further optimizations and characterization studies. However, this test is just one quality control test, and to ensure the overall quality and efficacy of the drug product, more Q.C. tests must be performed.⁴²

2.3 | Flow properties of SDSDs

2.3.1 | Carr index and Hausner ratio

The Carr indexes for AC1, AC2, and AC3 were 13.04%, 15.38%, and 14.28%, with Hausner ratios of 1.15, 1.18, and 1.16, respectively. All three batches were found to exhibit excellent/free flow as per these results, which were within the range of the Carr index (11–15%) and that of the Hausner ratio (1.12–1.18), indicating a free flow of powders.

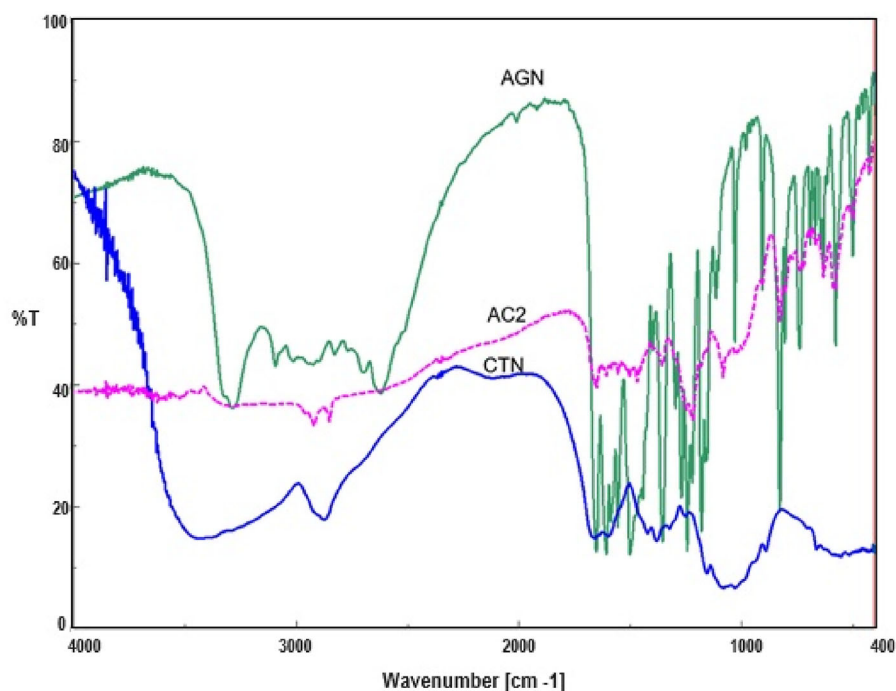


FIGURE 3 FTIR spectra of AGN, CTN, and AC2. [Color figure can be viewed at [wileyonlinelibrary.com](https://onlinelibrary.wiley.com/doi/10.1002/app.56310)]

2.3.2 | Angle of repose

The angle of repose indicates the degree of agglomeration or clustering of the particles in the powder. It is related to the interparticle forces and the powder's particle size distribution. The results for the SDSDs were found to be $22.3 \pm 0.14^\circ$, $20 \pm 0.21^\circ$, and $27 \pm 0.11^\circ$ for AC1, AC2, and AC3, respectively. All SDSDs were found to have good flow characteristics as the values of the angle of repose ranged between 20° and 30° .⁴³ By measuring the angle of repose of the SDSDs, one can determine whether the prepared product has the desired flow properties and whether the particle size distribution is suitable for the intended application, namely, filling a 3D printlet.

2.4 | FTIR spectroscopy

The FTIR spectrum (Figure 3) of apigenin typically shows peaks that represent the O-H stretching of the phenolic group (3285.14 cm^{-1}), C-H stretching of the aliphatic groups (3095.19 and 2619.82 cm^{-1}), C=O stretching of the carbonyl group (1668.48 cm^{-1}), C=C stretching of the aromatic ring (1613.1 cm^{-1}), C-H bending of the aromatic ring (1498.42 cm^{-1}), and C-O stretching of the carbonyl and ether groups (1243.86 – 1183 cm^{-1}).

The chitosan (CTN) spectrum exhibits several noteworthy peaks. At approximately 3441.35 cm^{-1} , there is a peak corresponding to the stretching vibration of the O-H and N-H groups in chitosan, indicating the presence of

hydrogen bonding. Another peak at 2666.67 cm^{-1} represents the stretching vibration of the C-H bonds in the chitosan backbone and the acetyl groups. Additionally, at 1665.23 cm^{-1} , there is a peak indicating the stretching vibration of the C=O bond in the acetyl groups. The amide bond (C=O and N-H) in the chitosan backbone is represented by a peak at 1378.85 cm^{-1} , corresponding to its stretching vibration. Furthermore, a peak at 1151.29 cm^{-1} suggests the bending vibration of the CH₃ groups in the acetyl groups. Another noteworthy feature is a broad peak at 1023.05 cm^{-1} , which corresponds to the stretching vibration of the C-O-C bond in the chitosan backbone. These spectral characteristics provide valuable information about the molecular structure and functional groups present in chitosan.

In the FTIR spectrum of a SDSD of chitosan apigenin (AC2), bands were visible corresponding to the stretching and bending vibrations of CTN (such as the amide bands at around 1650.77 cm^{-1} and 1465.63 cm^{-1}), as well as bands corresponding to the functional groups present in AGN (such as the aromatic ring vibrations at around 1223.61 cm^{-1} and the carbonyl group at around 1959.57 cm^{-1}). Apart from these, many individual peaks exhibited in AGN and CTN were present in AC2 without any significant modifications, indicating AGN and CTN were compatible with each other and did not show any physicochemical interactions and formation of a new bond or compound. FTIR spectroscopy is a valuable tool for analyzing chemical compounds and can provide important information on their composition, structure, and interactions.

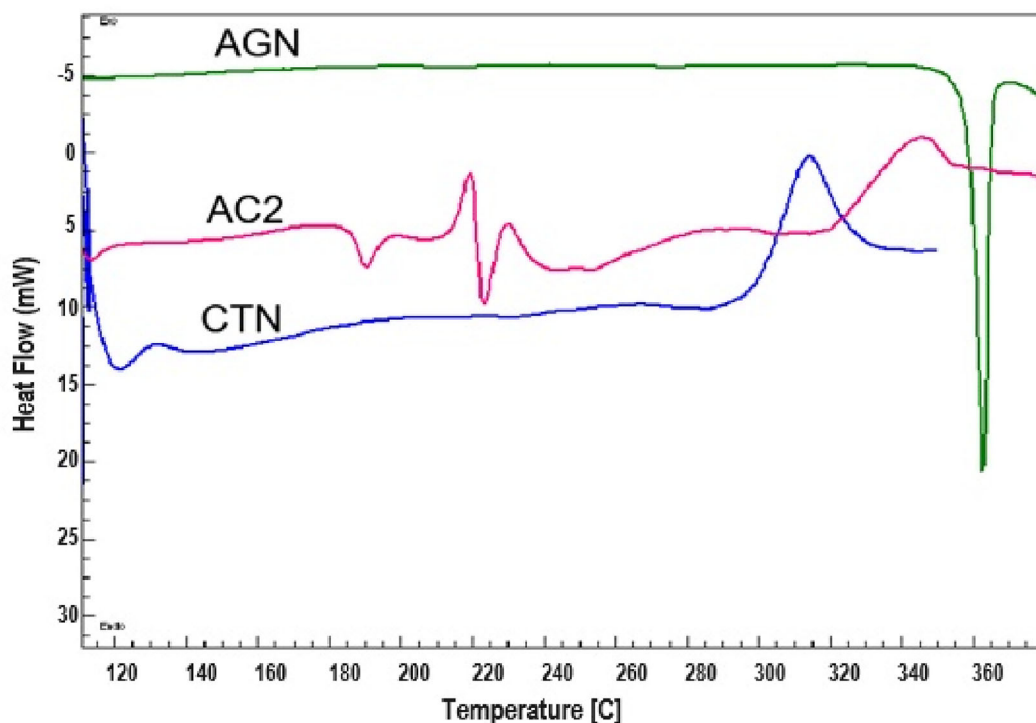
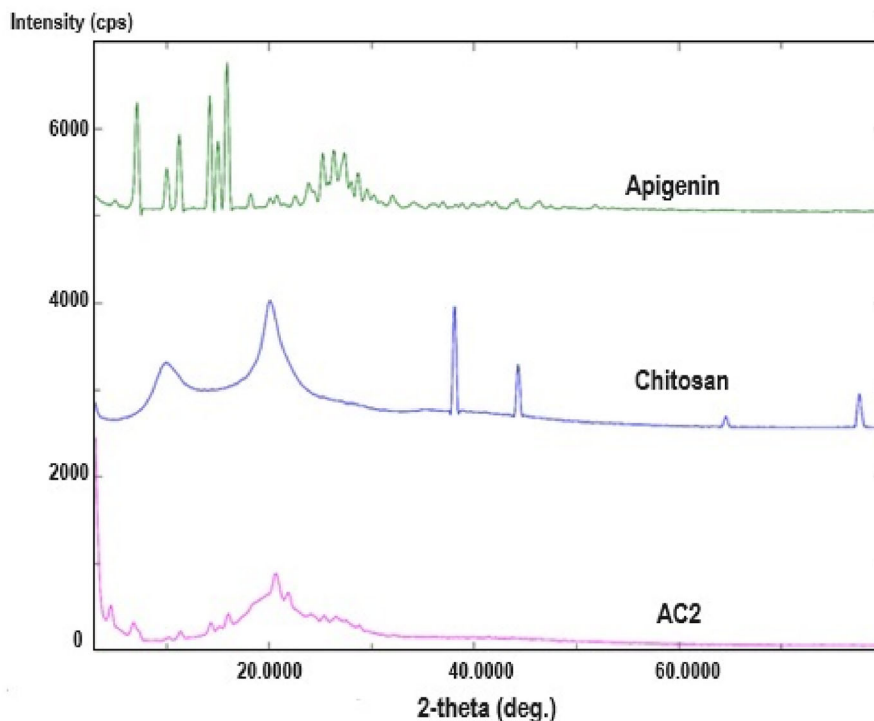


FIGURE 4 DSC thermograms of AGN, CTN, and the SDS AC2. [Color figure can be viewed at [wileyonlinelibrary.com](https://onlinelibrary.wiley.com/doi/10.1002/app.56310)]

FIGURE 5 X-ray diffraction patterns of AGN, CTN and the SDS AC2. [Color figure can be viewed at [wileyonlinelibrary.com](https://onlinelibrary.wiley.com/doi/10.1002/app.56310)]



2.5 | Differential scanning calorimetry

The DSC thermogram of AGN typically shows a single endothermic peak at 365°C, the corresponding melting point of the flavonoid compound. Chitosan's thermal

peak was observed at 110°C due to the melting transition indicated by a sharp endothermic peak, which could shift and corresponded to the deacetylation and the molecular weight of the polymer used in the study (Figure 4). This exothermic peak observed in chitosan is associated with

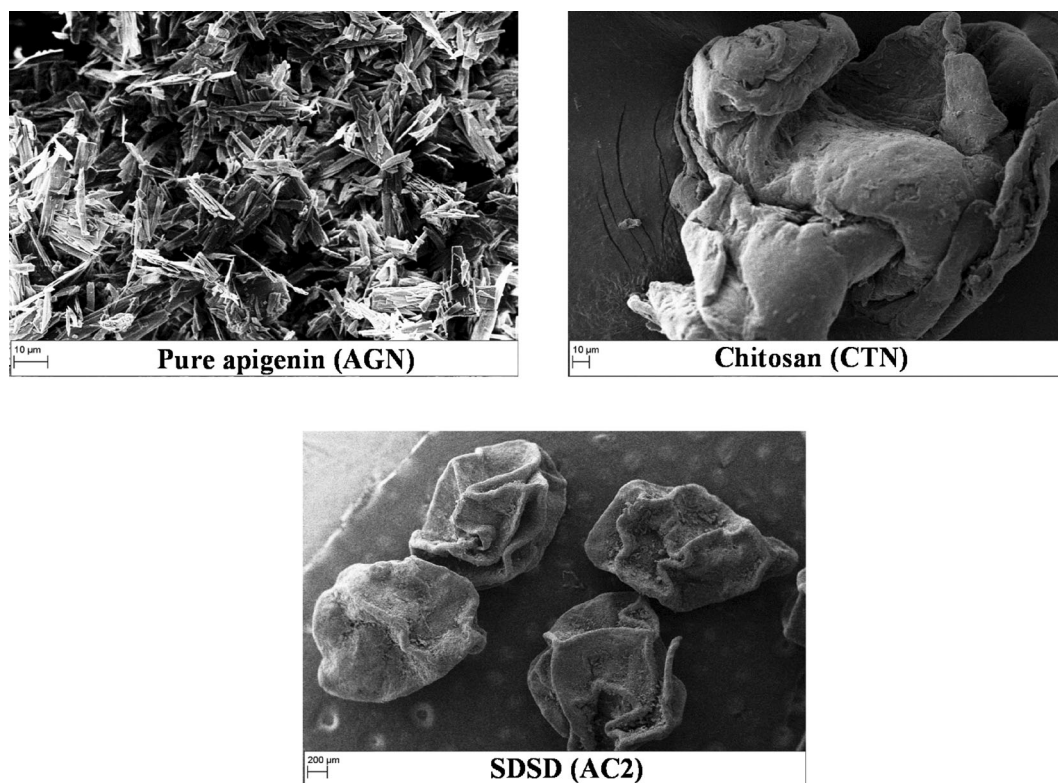


FIGURE 6 SEM images of apigenin (AGN), Chitosan (CTN), and SDS (AC2).

the decomposition of the chitin/chitosan macromolecule chain. At higher melting temperatures $>315^{\circ}\text{C}$, CTN begins to decompose. The thermogram of the SDS AC2 did not have any intense exothermic or endothermic peaks, indicating AGN was molecularly dispersed within the CTN, this is a desirable property of SDs reflecting the amorphousness of the prepared product.⁴⁴

2.6 | X-ray crystallography

The X-ray diffraction pattern of AGN showed diffraction peaks at 2θ values of 5.8° , 11.4° , 12° , 14° , 16.5° , 18.4° , 22.3° , and 26.4° , suggesting a crystalline structure with a monoclinic space group form of the flavonoid (AGN) used in this study (Figure 5). CTN exhibited broad peaks at around 2θ values of 10 and 20° , indicating a mixture of chitosan's crystalline and amorphous or disordered nature. Additional peaks were seen at 38° and 42° due to the degree of deacetylation and the material's crystallinity. In the diffractogram of SDS AC2, the peaks of both chitosan and apigenin were expected to be present, but their intensities were reduced with a shift in positions. A reduction in the intensities of the peaks indicates the solid state of the product is available in a less crystalline form and the presence of few peaks—typically a few percent of crystalline forms.

2.7 | Scanning electron microscopy

The SEM image of pure apigenin (AGN) reflected distinct and well-defined crystal structures. The SEM analysis provided visual evidence of the crystal morphology, revealing the presence of clear, sharply defined crystals of AGN. The CTN image showed porousness and rough shape, whereas the SDS AC2 showed a spherical shape with a shriveled surface that was wrinkled or uneven (Figure 6). The magnification scale for both AGN and CTN was $10\ \mu\text{m}$ whereas for AC2, it was $200\ \mu\text{m}$.

2.8 | Antimicrobial assay

A prepared SDS of AGN (AC2) was assessed for antimicrobial test against the different microflora of Gram-positive (*S. Aureus*, *B. subtilis*), Gram-negative (*E. coli*), and fungi (*C. Albicans*) in order to check its effectiveness on a broad spectrum. The zone of inhibition of AC2 was compared with the pure AGN to ensure the developed SDS had more therapeutic potential. The larger the zone of inhibition, the more effective the antimicrobial agent is against the microbe. For *S. Aureus*, both AGN and AC2 showed good activity with zone-zone inhibition values of 17 ± 1.47 and $19 \pm 1.65\ \text{mm}$, respectively. Similarly, for *B. subtilis*, the two agents demonstrated a

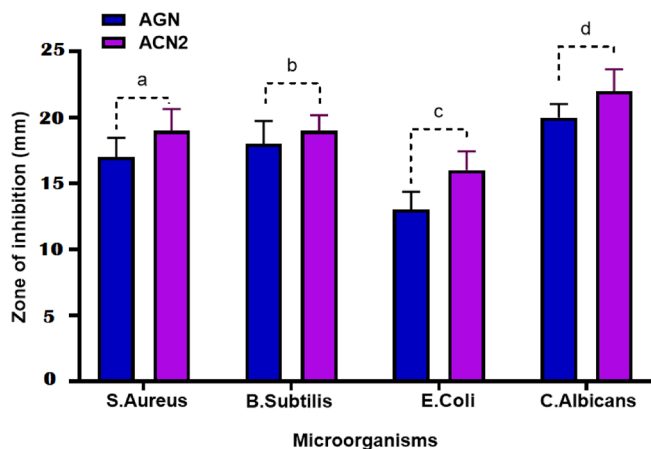


FIGURE 7 Zone of inhibition (mm) of AGN and the SDSD AC2 against different microbial strains, wherein; $a = 0.7388$, $b = 0.8694$, $c = 0.5776$, and $d = 0.7576$ for the two-sided p -value. [Color figure can be viewed at wileyonlinelibrary.com]

similar activity with a zone of inhibition of 18 ± 1.75 and 19 ± 1.18 mm, respectively. However, for *E. coli*, both AGN and AC2 demonstrated a lower activity with a zone of inhibition of 13 ± 1.38 and 16 ± 1.43 mm, respectively (Figure 7). This suggests these agents may not be as effective against this strain as the others.

On the other hand, for *C. Albicans*, both AGN and AC2 showed a good activity with a zone of inhibition of 20 ± 1.03 and 22 ± 1.63 mm, respectively. This indicates that these agents are highly effective against this fungal strain. The results suggest that AGN and AC2 have varying degrees of antimicrobial activity against different strains of microorganisms; AC2 was more effective against pure AGN. Osonga et al. suggested AGN derivatives showed strong antibacterial effects against Gram-negative compared to Gram-positive bacteria.⁴⁵ Published reports suggested that AGN exerted an antibacterial and antifungal activity by inducing membrane disturbances, leading to cell shrinkage, leakage, and organism death.⁴⁴

2.9 | Antioxidant activity

The antioxidant activity analysis was performed for pure flavonoid (AGN) and the AC2 SDSDs, at concentrations of 200–1000 ppm; the DPPH scavenged activity was found to be in the range of 39.31 ± 2.32 – $61.6 \pm 11.32\%$ for pure AGN and for SDSDs, it was noted to be 45.34 ± 1.65 – $92.32 \pm 1.76\%$. AGN has a natural antioxidant activity due to its flavonoid property; therefore, pure AGN showed an antioxidant activity. However, the AC2 SDSDs have increased antioxidant effects due to the synergistic effects of AGN and CTN. Chitosan is a natural polymer derived from chitin, found in the exoskeletons of crustaceans such

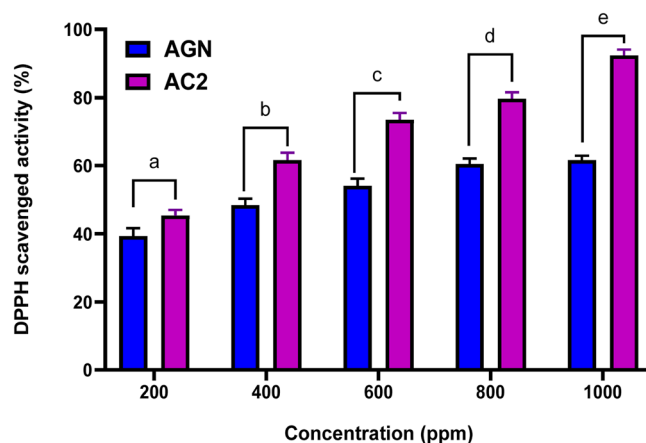


FIGURE 8 Antioxidant effect of AGN and the SDSD AC2 at different concentrations, –; $a = 0.51$, $b = 0.20$, $c = 0.08$, $d = 0.10$, and $e = 0.01$ for the two-sided p -value. [Color figure can be viewed at wileyonlinelibrary.com]

as shrimp and crabs. Chitosan has been shown to have antioxidant properties as well. More studies have reported that combining apigenin and chitosan may enhance the antioxidant activity of both compounds. Zafar et al. investigated the chitosan-based nanoparticles loaded with APG, and results showed an enhanced antioxidant activity.⁴⁵ However, more research is needed to fully understand the mechanisms underlying this effect and determine the optimal ratios and concentrations of the two compounds for maximizing their antioxidant potential. The antioxidant mechanism of AGN may involve one or more pathways such as chelating metal ions to stop the formation of reactive oxygen species, increasing the expression of superoxide dismutase, and suppressing the NADPH oxidase and xanthine oxidase enzymes. AGN also scavenges free radicals such as superoxide anions, hydroxyl radicals, and peroxy nitrite, thereby donating hydrogen atoms to the free radicals, thereby neutralizing them and preventing oxidative damage to cells. However, chitosan has been reported to show an antioxidant activity in addition to the aforementioned process. via the inhibition of lipid peroxidation, a process in which free radicals attack the unsaturated fatty acids in cell membranes by neutralizing the lipid-derived free radicals.

CTN, despite having an unshared pair of electrons on its N-atom that could potentially be donated, has a pK_a of approximately 6.3. In solution, where the polymer needs to be acidified to dissolve, the amino groups of CTN are predominantly protonated, rendering them unable to donate electrons. Additionally, chitosan lacks a hydrogen atom that can be easily donated in order to serve as a good antioxidant.⁴⁶ A plot of the percentage of DPPH scavenged against the concentration of the test sample AC2 and AGN is given in Figure 8.

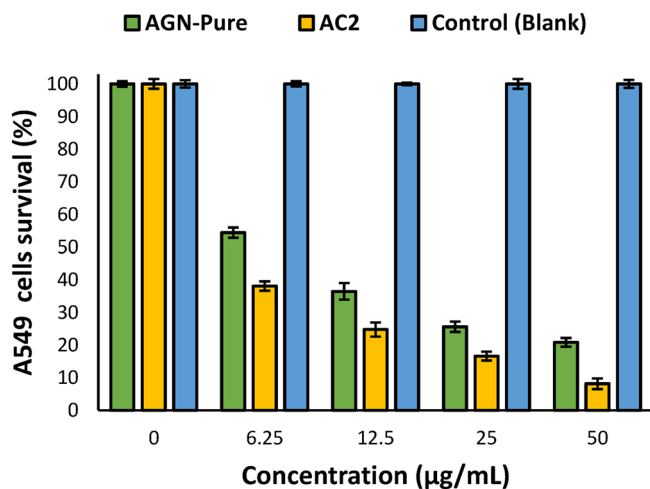


FIGURE 9 Antiproliferative effect of AGN and the SDDS AC2 against A545 lung cancer cell lines. [Color figure can be viewed at [wileyonlinelibrary.com](https://onlinelibrary.wiley.com/doi/10.1002/app.56310)]

2.10 | Antiproliferative activity

The percentage of viability of the A549 cells of the AC2 SDDS was found to be $38.15 \pm 1.45\%$, $24.79 \pm 2.16\%$, $16.64 \pm 1.34\%$, and $8.15 \pm 1.64\%$ compared to pure AGN (54.46 ± 1.56 , 36.51 ± 2.54 , 25.64 ± 1.59 , and $20.84 \pm 1.35\%$) at concentrations of 6.25, 12.5, 25, and 50 µg/mL. At the tested concentration (50 µg/mL), both AGN-Pure and AC2 significantly reduced the viability of the A549 cells compared to the control group (0 µg/mL), indicating AGN was effective against lung cancer. AGN acts as an antiproliferative agent by activating the apoptosis pathway that decreases the PI3K/Akt signaling pathway, triggering cancer cell death and preventing lung tumors.^{18,47–49} The half-maximal inhibitory concentration (IC₅₀) was also calculated, indicating the concentration of a flavonoid (AGN) and AC2 SDDS product needed to inhibit the growth of cancer cells by 50%. AC2 had an IC₅₀ value of 3.7707, which was relatively lower than the IC₅₀ value of AGN-Pure, which was 5.3979. In that case, AC2 had an IC₅₀ value of 3.7, lower than the IC₅₀ value of AGN-Pure, which was 5.3. This indicates that AC2 is more potent than AGN-Pure in inhibiting the growth or proliferation of cancer cells. These values suggest that AC2 is more potent than AGN-Pure in inhibiting the biological activity or process being studied (Figure 9).

Therefore, the AC2 SDDS could be a potential cell proliferation inhibitor by interfering with the cell-cycle regulation at different phases, such as G1 or G2/M; it is effective in lung cancer treatment wherein the PI3K/Akt pathway is often overactivated, leading to increased cell survival and resistance to apoptosis. By inhibiting PI3K,

AGN reduces the activation of Akt (protein kinase B), a key mediator of cell survival and proliferation. This leads to decreased cell survival signals and an increased susceptibility to apoptosis. Moreover, AGN can modulate multiple proteins involved in apoptosis, including Bcl-2 family members, caspases (proteases involved in apoptosis), and p53 (a tumor suppressor protein).

2.11 | Fabrication of 3D-printed PVA Shell pill

The 3D-printed PVA shell-pill fabrication is an innovative approach to creating a capsular shell-pill design using prefabricated PVA filaments and a 3D printer. This method allows the creation of complex geometries that would be difficult or impossible to achieve using traditional manufacturing methods.

One of the key advantages of this approach is that the fabricated shell could be used to store/fill the SDDS of AGN (AC2) with precision and accuracy, with an equivalent of 50 mg of AGN, a reported daily dose of flavonoid (AGN). The shell pill was filled with 125 mg of AC2. The capsular shell-pill design allows for the sustained release of AGN, which can even be tailored by adjusting the filling amount to meet specific patient needs. This makes it an ideal solution for personalized medicine and drug delivery. Using prefabricated PVA filaments also simplifies manufacturing, eliminating the need for complex tooling and molds. This reduces production costs and lead times, making it a more efficient and cost-effective solution. This innovative approach holds promise for the development of novel drug delivery systems and advancements in the field of pharmaceuticals.

2.12 | Dissolution profile and release kinetic

The dissolution profiles of pure AGN and the AC2 3D shell pill are compared in Figure 10. The study results indicate that the shell pill exhibited a burst release of AC2 after 30 min, with a percentage of $22.76 \pm 0.74\%$, whereas the pure AGN showed a lower burst release of $7.98 \pm 0.77\%$. This pattern of therapeutics, characterized by an initial quick release followed by a more sustained release, offers advantages in maintaining the optimal blood concentration of the medication in patients.⁴²

Over time, the active moieties in both dissolution baskets exhibited distinct release rates. Approaching the 24 h mark, the pure AGN showcased a release of $25.47 \pm 0.46\%$, whereas the AC2 3D shell pill released $86.73 \pm 2.64\%$. A remarkable improvement of 2.40 folds in drug

release was observed from the AC2 3D shell pill compared to the pure AGN. Furthermore, the inclusion of AGN-CTN may further enhance the efficacy of AGN. CTN possesses mucoadhesive properties and the ability to open tight junctions, thereby enhancing permeability across the gastrointestinal (GI) tract. The kinetics models proposed for the release mechanism revealed a correlation coefficient R^2 of 0.68 (zero order), 0.91 (first order), 0.90 (Higuchi model), and 0.96 (Korsmeyer–Peppas), respectively. Based on the (R^2) the Korsmeyer–Peppas model was considered the best-fitted model for the AC2 SDS-filled shell pill.

The Korsmeyer–Peppas model is an empirical model to describe the drug release from flavonoid–polysaccharides (AGN-CTN) matrices. It can be used to describe various types of release kinetics, including Fickian diffusion, non-Fickian release, and case II transport. Moreover, the model allows for the determination of the release mechanism by the diffusion exponent n with a value of 0.288. This suggests that the release mechanism is non-Fickian or an anomalous diffusion, indicating that factors such as swelling or erosion of the CTN matrix or the presence of channels or pores in the matrix may contribute to the AGN release process.

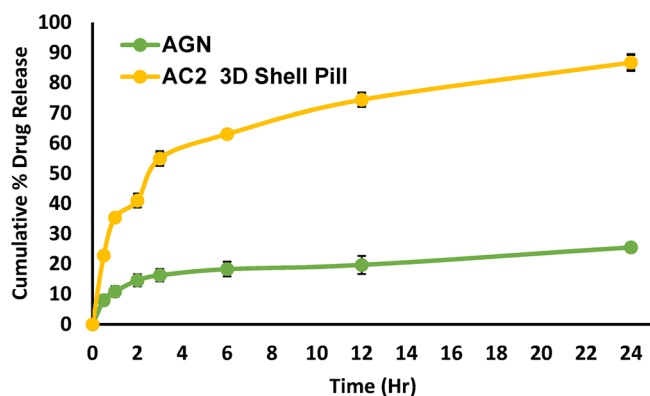


FIGURE 10 Dissolution profile of AGN and a shell pill filled with AC2 SDS. [Color figure can be viewed at wileyonlinelibrary.com]

2.13 | Stability studies

The stability study results indicated that the two dissolution profiles before and after stability of the AC2 SDS-filled 3D shell pill had highly similar drug release profiles over time with a similarity index (f_2) of 51.52. This was supported by a strong positive correlation Pearson coefficient of approximately 0.9949 between the two dissolution profiles (Figure 11). The drug release data showed that both shell pills gradually increased the cumulative percentage of drug release over time.

3 | MATERIALS AND METHODS

3.1 | Materials

Apigenin (mol. wt.: 270.24 g/mol) was obtained from Beijing MesuChem Technology Co. Pvt. Ltd. (Beijing, China). Chitosan (50,000 g/mol) and the culture medium Dulbecco's modified Eagle's medium (DMEM) were obtained from Sigma (St. Louis, MI, USA), supplemented with FBS, which supports the growth of A549 cells and was used in the antiproliferation studies. Poly vinyl alcohol (PVA) a colorless printing filament, with a diameter of 1.75 ± 0.05 mm, and print temperature range of 180–205°C was purchased from Sigma-Aldrich Chem Pvt. Ltd., Bangalore. Solvents and other chemicals were of analytical grades, purchased from Fine Chemicals.

3.2 | Preparation of chitosan-based spray-dried solid dispersions (SDSDs) of apigenin

Apigenin-encumbered SDSDs were prepared using chitosan by the spray-drying technique. Flavonoid and polysaccharide ratios of 1:1 (AC1), 1:1.5 (AC2), and 1:2 (AC3) w/w (g/g) were selected for the preparations of apigenin–chitosan SDSDs. Chitosan (1,1.5 and 2 mg) was first

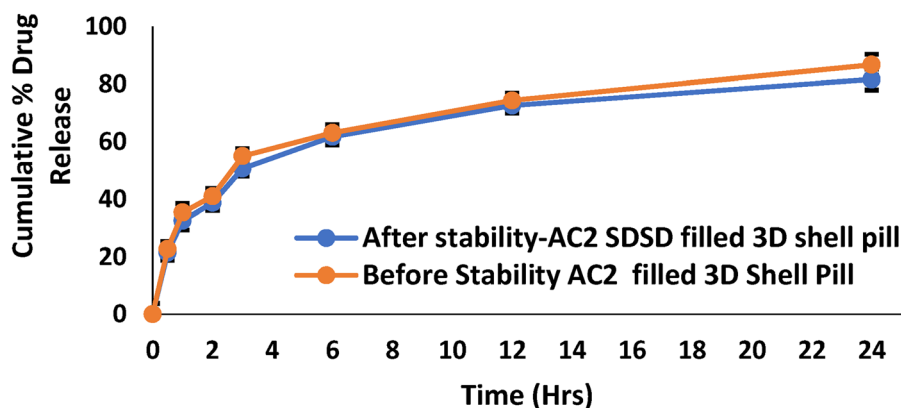


FIGURE 11 Before and after dissolution profiles of the 3D shell pill filled with the AC2 SDS. [Color figure can be viewed at wileyonlinelibrary.com]

dissolved in (40 mL) aqueous acetic acid 1% (v/v) separately; the mixtures were then kept on a magnetic stirrer overnight to obtain a homogenous solution. The required amount of AGN (1 mg) was dissolved into the ethanol (60 mL) and ultrasonicated for 2 min to complete the dissolution. Aqueous (chitosan solution) and organic (AGN solution) solutions were then mixed in a proportion of 60:40. Both solutions were homogenized by a high-speed homogenizer (Wiggins GmbH; model: D-500, accessories: SS20FER20, Gässlesweg, “made in Germany”). The AGN-CTN dispersion was pumped into the spray dryer (Buchi Mini Spray Dryer, Model-B-290, Flawil “made in Switzerland”). The parameters optimized were the inlet temperature (80°C), aspiration (90%), and flow rate (15 mL/min), in a nitrogen environment (28–30 flow rate). The process involved the sprinkling of the dispersion through the nozzle (0.5 mm) in a hot-air chamber, and the dried powder formed was passed through a cyclone separator and was collected into the jar. The prepared SDSDs were then preserved in the glass vials till further studies.^{30,31,34,49–51}

3.3 | Process yield percentage

Spray-drying technology involves various unit operations: weighing, mixing, homogenization using a thermostatically controlled magnet stirrer (100 RPM), and drying. Therefore, the loss of materials (products) needs to be calculated to confirm that the product is economical and the process is optimized. The product (SDSDs AC1-3) and the precursors' (AGN and CTN) weights were considered to calculate the process yield (Equation 1).³⁰ The success of the manufacturing/product depends on the yield (%).

$$\text{Process yield (\%)} = \frac{\text{Weight of SDASD}}{\text{Weight of CTN} + \text{weight of AGN}} \times 100 \quad (1)$$

3.4 | Drug assay

The developed SDSDs containing an equivalent amount of AGN (5 mg) were dissolved in aqueous ethanol and mechanically agitated for 24 h under a controlled environment at $25 \pm 0.5^\circ\text{C}$. The aliquots were then prefiltered through a $0.22 \mu\text{m}$ syringe filter and analyzed for drug content using ultraviolet spectroscopy at a λ_{max} of 272 nm (Jasco spectrophotometer V-630, Tokyo, “made in Japan”). The absorbance of the test was compared with the standard, and the concentration (%) was calculated.⁵²

3.5 | Flow properties of SDSDs

3.5.1 | Carr index and Hausner ratio

Bulk and tapped density were measured by charging the weight amount of SDSDs (AC1-3) in the measuring cylinder, noting down its volume (bulk volume), followed by tapping it in a Pharma Test apparatus (PT-TD200; Hainburg, “made in Germany”) to obtain the tapped volume. We calculated the density (ρ) from weight/volume and computed the values in the equations to get the Carr index (Equation 2) and Hausner ratio (Equation 3). Both Carr index and Hausner ratio are two preformulation parameters used to evaluate the flow properties of powders. The Carr index indicates flowability, whereas the Hausner ratio provides the compressibility of prepared SDSDs. A low Carr index and Hausner ratio are required to better fill the selected batch into the 3D printlet.

$$\text{Carr index} = \frac{\rho_{\text{tapped}} - \rho_{\text{bulk}}}{\rho_{\text{tapped}}} \times 100 \quad (2)$$

$$\text{Hausner ratio} = \frac{\rho_{\text{tapped}}}{\rho_{\text{bulk}}} \quad (3)$$

3.5.2 | Angle of repose

The angle of repose is a parameter that can be used to evaluate the flowability and cohesion of prepared SDSDs (AC1-3). The flow ability of the powders can also be determined by the angle of repose in which the powder is allowed to flow through a funnel, it falls on the surface, and the height (h) and radius (r) of the sample heap were measured by laser and the result θ was printed. A Pharma Test automated powder flow analyzer was used (PharmaTest PTG-S4 Hainburg Germany) to measure the angle of repose (θ) (Equation 4 θ is an angle between the surface of the pile and the horizontal plane).³⁷

$$\theta = \text{Tan}^{-1}h/r \quad (4)$$

3.6 | FTIR spectroscopy

A compatibility test was performed using Fourier transform infrared (FTIR) spectroscopy (Jasco FTIR spectrophotometer, Tokyo, “made in Japan”). AGN, CTN, and selected batch SDSDs (AC2) based on the yield and drug content were individually triturated with KBr. The IR dispersion was then compressed to a pellet and kept in the Fourier transform (FT) spectroscope to generate the spectrums within the fingerprint region of the molecules from 4000 to 400 cm^{-1} . The spectrums were interpreted for the possible chemical interactions between CTN and AGN.⁵³

3.7 | Differential scanning calorimetry

A thermal analysis of samples (CTN, AGN, and AC2 SDSDs) was performed by cramping (5 mg) the sample in an aluminum hemispherical pan. The test pan was kept beside the reference (empty) pan. The temperature was then raised from 40 to 350°C at a 20°C/min heating rate under nitrogen conditions (40 mL/min). Thermograms of all the samples were analyzed, collaged using software, and interpreted (Scinco, DSC N-650, Seoul, “made in Korea”).⁴⁹ The endothermic peak of AGN was then traced to note down the m.p of the flavonoid.

3.8 | X-ray crystallography

The crystallography study was performed by an Ultima IV diffractometer (Rigaku Inc. Tokyo “made in Japan”), operated at a voltage/current (40 kV/40 mA) using a Cu K α radiation, scanned with a speed of 0.500 deg./min in the range from 3 to 50 Å (2 θ). The samples (AGN, CTN, and SDSDs AC2) were analyzed for Bragg's peaks.⁵⁴

3.9 | Scanning electron microscopy

The morphological features of the materials used (CTN, APN, CA2 SDSDs) were examined using a coating technique. The samples were coated onto glass slides (5 nm) that were precoated with a layer of gold. The coating process involved applying a current of 20 mA for a duration of 2 min. Under the negative pressure, the sample was bombarded with an electron beam, and scanned coarse and fine imaging adjustments were performed to capture the required zone, shape, and size. With an operation at 5 kV with a distance of 8–10 mm, images were obtained by scanning and magnification (SEM-Ultraplus, Zeiss, “made in Germany”). This technique allowed for the visualization and analysis of the material's morphology under the electron microscope.

3.10 | Antimicrobial assay

Gram-positive bacteria (*Staphylococcus aureus*, *Bacillus subtilis*), gram-negative bacillus (*Escherichia coli*), and a pathogenic fungal strain (*Candida albicans*) were used in this study. The composition of bacterial culture included a nutrient broth composed of peptic digest, yeast, and beef extract fungal growth medium containing Sabouraud dextrose. The growth medium after sterilization was poured into Petri plates after solidification, they were inoculated with microbial strains, and the sample well

was bored and filled with AC2 suspension. The plates were incubated and examined for the zone of inhibition.^{55–57}

3.11 | Antioxidant activity

The antioxidant effects of AGN, SDSDs (AC2), and ascorbic acid was performed using the 2,2'-diphenyl-1-picrylhydrazyl test (DPPH). This assay uses the DPPH radical, a stable free radical with a deep violet color, as a model oxidizing agent. Reference standards were prepared by dissolving DPPH in methanol (0.1 mM) and the concentration was then diluted further to 1–100 g/mL. The samples under investigation were also prepared in a serial dilution. The test mixture was then prepared by 0.5 mL (sample) individually into 2 mL of a 0.1 mM DPPD methanol solution (0.5 mL). The reaction was allowed between the sample and DPPH for about a half-hour in dark conditions at room temperature (25°C).

When an antioxidant (AGN and SDSD-AC2) is added to a DPPH solution, it can donate an electron or hydrogen atom to the DPPH radical, reducing its color intensity. This reduction in color intensity can be measured spectrophotometrically and is used as an indication of the antioxidant activity of the compound (Equation 5). A higher percentage of DPPH scavenged by the compound indicates a higher antioxidant activity.⁵⁸ The absorbance (A) of the test sample (Test) and standard (STD) was taken at a λ_{max} of 517 nm using a UV spectrophotometer (Jasco, modelV 630, Tokyo made in Japan).

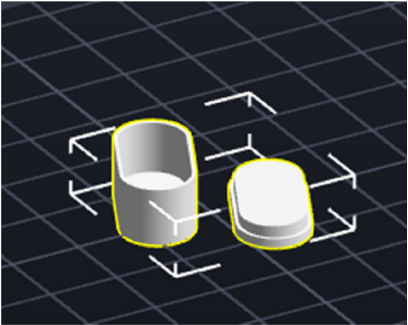
$$\text{Antioxidant effect (\%)} = \frac{A_{517\text{STD}} - A_{517\text{Test}}}{A_{517\text{Test}}} \times 100 \quad (5)$$

3.12 | Antiproliferative activity

An apigenin–chitosan spray-dried solid dispersion was tested against the A549 lung cancer cell lines using an MTT assay. The selected cell line was cultured in a medium composed of Dulbecco's modified Eagle's medium (DMEM) encompassing 10% fetal bovine serum (FBS), and antibiotics (1% penicillin/streptomycin) added to prevent bacterial contamination from both Gram-positive and Gram-negative bacteria. Glutamine (2 mM) and insulin (0.01 mg/mL) were added to support and facilitate the cell growth, which required a large quantity of proteins and nucleic acids.^{59,60}

After the 70–80% confluence of cell lines (A549) treated with the AC2 SDSDs and pure AGN at different concentrations of (0, 6.25, 12.5, 25, and 50 $\mu\text{g/mL}$), we measured the ability of the cells to convert a colorless substrate into a purple formazan, which has a maximum

TABLE 1 PVA filament-based shell-pill design parameters.

STL file	Slicing parameters		Printing parameters	
	Layer thickness	0.2 mm	Printing temperature	200°C
	Shell thickness	1.2 mm	Bed temperature	60°C
	Initial layer thickness	0.3 mm	Printing speed	60 mm/s
	Infill density	15%	Travel speed	80 mm/s
	Adhesion	Raft	Bottom speed	20 mm/s

Capsular shell-pill body and cap

absorbance at 570 nm, using a spectrophotometer. The absorbance is proportional to the number of viable cells. The data obtained were analyzed statistically to determine the significance of the antiproliferative activity of apigenin against A549. IC₅₀ was also calculated using the Quest Graph™ IC₅₀ calculator.

3.13 | Fabrication of 3D-printed PVA Shell pill

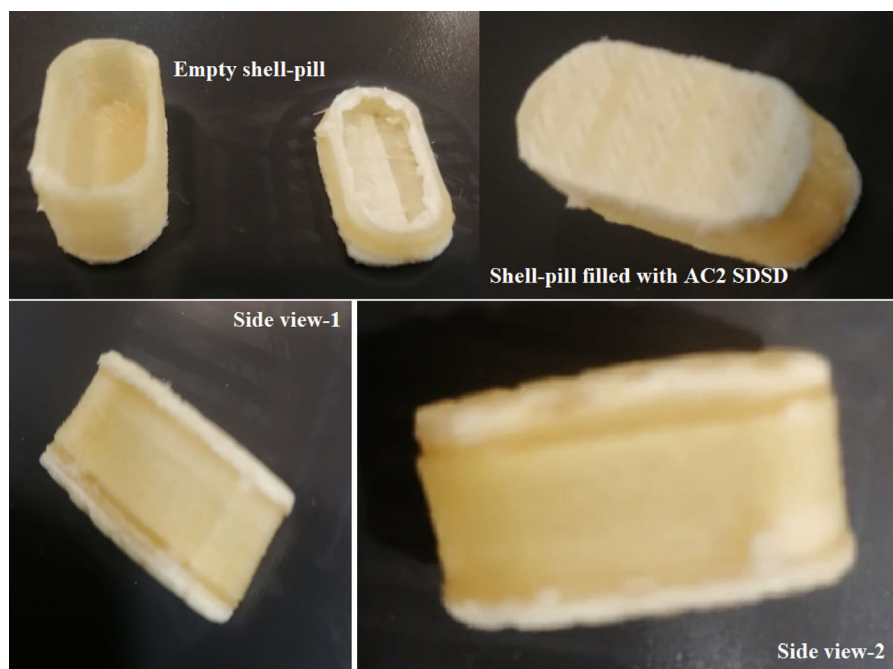
Prefabricated PVA filaments were used to fabricate an FDM-based 3D-printed shell pill. In order to fill the SDS of AGN (AC2), a capsular shell-pill design was printed using a 3D printer (Easithread X1 Model, “made in China”) with a heating stage.⁶¹ The shell pill’s geometry was designed using computer-aided software Autodesk Fusion 360. The 3D capsular shell pill was printed in an oblong shape with a cap and a body. The shell body was filled with AC2, and the cap was placed over it to seal the shell. The dimension of the capsular shell body was 20 mm in length and 10 mm in width, with an 8 mm inner depth, and the shell cap was 20 mm in length and 10 mm in width with a 3 mm inner layer depth to be fixed on the body. The shell design was saved as an STL (Standard Triangle Language) file, which describes the 3D geometry of the design (Table.1). This STL file was transferred to 3D printer software which converted it to printer-readable G-code (geometric code for computer numerical control). The G-code for the designed 3D shell was formed by using 3D printer slicer software Repetier-Host V2.2.4 (with Slic3r Slicer). This G-code comprised all the slicing details for the design and printing parameter settings for the printer. The layer thickness, shell thickness, and initial layer thickness were set to 0.2, 1.2, and 0.3 mm, respectively. The infill density was 15% with a rectilinear infill. The printing, travel, and bottom speeds were set to 60, 80, and 20 mm/s, respectively. The

low printing speed at the bottom facilitated the adhesion of the initially printed layers to the print bed. The PVA filament was fed into the extruder of the 3D printer, wherein the filament got melted and extruded through the nozzle over a build plate and formed the designed 3D shell pill in a layer-by-layer pattern.⁶² The diameter of the loaded PVA filament was 1.75 mm, and the extruder’s nozzle size was 0.4 mm. The nozzle temperature was set to 200°C, and the bed temperature to 60°C. After printing, the capsular shell body and cap were removed from the printer bed, separated from the raft support, filled with AC2, and subjected to further characterization (Figure 12). The printing was carried out without retraction.⁶³ PVA filament-based shell-pill design parameters are summarized in Table 1.

3.14 | Dissolution profile and release kinetic

An apigenin–chitosan SDS (AC2) with an equivalent weight of 50 mg of AGN filled in the 3D printed shell pill was placed into the basket (USP-II), filled with medium, dissolved in 900 mL of gastric fluid with a pH 3 phosphate buffer. Another flask was added with pure AGN (50 mg) filled in a PVA shell pill. Both flasks were immersed into the water jacket maintained at $37 \pm 0.5^\circ\text{C}$ (Erweka-disso DT950, Langen, made in Germany). At predetermined intervals, aliquots of 1 mL were withdrawn from each flask and replenished with the fresh medium. Samples were analyzed for the AGN released percentage; the data were then filtered to the release kinetics models to calculate the release mechanism. The drug quantification was performed by using UV spectroscopy (Jasco V-630, Tokyo, “made in Japan”) at λ_{max} of 272 nm. Release data were computed using the mathematical equations of the zero-order, first-order, Higuchi, and Korsmeyer–Peppas models.

FIGURE 12 PVA filament-based shell pill filled with AC2 SDS. [Color figure can be viewed at wileyonlinelibrary.com]



3.15 | Stability studies

An AGN-filled PVA shell pill was exposed to $40 \pm 0.5^\circ\text{C}$, with a relative humidity of 75%; the pill was kept for 90 days, and a release study was performed as discussed in the above section. We performed a before and after stability test, and the release data were added to the similarity index (f_2) (Equation 6). f_2 stands for similarity index, n is the dissolution time, R_t and T_t are reference and test dissolutions at time t .⁶² According to SUPAC guidelines, if the difference between the release data is ≤ 50 , it indicates that the products exhibit similar drug release characteristics, and the storage conditions do not significantly impact the fabricated pill.

$$f_2 = 50 \times \log \left\{ \left[1 + \frac{1}{n} \sum_{t=1}^n (R_t - T_t)^2 \right] - 0.5 \times 100 \right\} \quad (6)$$

Similarity, a metric such as the Pearson correlation coefficient was also calculated for both release profiles of the AC2 3D shell pill.

3.16 | Statistics and software

Microsoft Excel 2016 was used in the release rate and similarity index calculations. The software tool used for the design of the 3D pill was Fusion 360. The analysis was performed using an ANOVA (analysis of variance) and results with $p < 0.05$ were considered significant. GraphPad Prism 8.0.2 software was also used for generating the graph presented in this publication. All the

parameter calculations were performed, and the results were obtained with $n = 3$.

4 | CONCLUSIONS

This study suggests that chitosan-based spray-dried solid dispersions of apigenin show an improved drug release, enhanced antimicrobial activity, antioxidant properties, and potential anticancer effects in A549 lung cancer cell lines. The researchers utilized three different ratios (1:1, 1:1.5, and 1:2) of apigenin inclusion in chitosan, performed a characterization of the resulting solid dispersions, and conducted physicochemical and pharmacological evaluations. The selected solid dispersion (AC2) was further developed into a 3D-printed shell pill, providing a suitable formulation and dosage unit. The AC2 solid-dispersion-filled 3D shell pill demonstrated potential as a dosage unit for A549 lung cancer, potentially allowing for a personalized drug dosage and adjustment to meet individual patient needs. Overall, this study suggests that the apigenin–chitosan solid dispersion 3D-printed pill could serve as a promising therapeutic option with multiple beneficial properties. However, further research and testing are required to fully comprehend the potential benefits and limitations of this solid dispersion for various applications, as well as to evaluate its efficacy and safety in vivo.

AUTHOR CONTRIBUTIONS

M. Ali Aboudzadeh: Conceptualization (supporting); methodology (supporting); supervision (lead); validation (lead); visualization (lead); writing – review and editing

(supporting). **Amer S. Alali:** Investigation (lead); methodology (lead); writing – original draft (lead). **Mohammed Muqtader Ahmed:** Conceptualization (lead); funding acquisition (lead); resources (lead); validation (equal); visualization (equal). **Farhat Fatima:** Formal analysis (equal); investigation (supporting); methodology (equal); writing – original draft (supporting). **Md. Khalid Anwer:** Conceptualization (supporting); data curation (supporting); resources (supporting); validation (supporting); writing – review and editing (supporting). **Mutasim Ibauf:** Formal analysis (supporting); investigation (supporting); methodology (supporting); writing – original draft (supporting).

ACKNOWLEDGMENTS

The authors extend their appreciation to Prince Sattam bin Abdulaziz University for funding this research work through the project number (PSAU/2023/03/25933).

DATA AVAILABILITY STATEMENT

The data that support the findings of this study are available from the corresponding author (Mohammed Muqtader Ahmed) upon reasonable request.

ORCID

M. Ali Aboudzadeh  <https://orcid.org/0000-0001-8829-8072>

REFERENCES

- [1] D. Zhao, S. Yu, B. Sun, S. Gao, S. Guo, K. Zhao, *Polymer* **2018**, *10*, 462.
- [2] P. Baharlouei, A. Rahman, *Mar. Drugs* **2022**, *20*, 460.
- [3] S. Bandara, H. Du, L. Carson, D. Bradford, R. Kommalapati, *Nanomaterials* **1903**, *2020*, 10.
- [4] A. Pellis, G. M. Guebitz, G. S. Nyanhongo, *Gels* **2022**, *8*, 393.
- [5] S. Crognale, C. Russo, M. Petruccioli, A. D'annibale, *Fermentation* **2022**, *8*, 76.
- [6] M. A. Mohammed, J. T. M. Syeda, K. M. Wasan, E. K. Wasan, *Pharmaceutics* **2017**, *9*, 53.
- [7] X. Gong, Y. Gao, J. Shu, C. Zhang, K. Zhao, *Vaccines* **1906**, *2022*, 10.
- [8] M. M. Ahmed, K. Anwer, F. Fatima, A. S. Alali, M. A. Kalam, A. Zafar, S. Alshehri, M. M. Ghoneim, *Gels* **2022**, *8*, 253.
- [9] A. Zamboulis, S. Nanaki, G. Michailidou, I. Koumentakou, M. Lazaridou, N. M. Ainali, E. Xanthopoulou, D. N. Bikiaris, *Polymer* **2020**, *12*, 1519.
- [10] S. Shim, H. Yoo, *Mar. Drugs* **2020**, *18*, 605.
- [11] A. E. Caprificio, P. J. S. Foot, E. Polycarpou, G. Calabrese, *Pharmaceutics* **2020**, *12*, 1013.
- [12] M. Mohammed, M. S. Alnafisah, M. K. Anwer, F. Fatima, B. K. Almutairy, S. M. Alshahrani, A. S. Alshetaili, A. Alalaiwe, M. H. Fayed, A. Z. Alanazi, M. al Zahrani, M. M. Hailat, R. al-Shdefat, *J. Polym. Eng.* **2019**, *39*, 909.
- [13] K. Noorulla, M. Yasir, F. Muzaffar, S. Roshan, M. M. Ghoneim, A. S. Almurshedi, A. J. Tura, S. Alshehri, T. Gebissa, S. Mekit, *J. Drug Deliv. Sci. Technol.* **2021**, *67*, 102939.
- [14] K. Anwer, E. A. Ali, M. Iqbal, M. M. Ahmed, M. F. Aldawsari, A. Saqr, A. Alalaiwe, G. A. Soliman, *Processes* **2022**, *10*, 1329.
- [15] B. Salehi, A. Venditti, M. Sharifi-Rad, D. Kregiel, J. Sharifi-Rad, A. Durazzo, M. Lucarini, A. Santini, E. B. Souto, E. Novellino, H. Antolak, E. Azzini, W. N. Setzer, N. Martins, *Int. J. Mol. Sci.* **2019**, *20*, 1305.
- [16] J. H. Yoon, M.-Y. Kim, J. Y. Cho, *Int. J. Mol. Sci.* **2023**, *24*, 1498.
- [17] R. Ranjan, K. Kishore, S. Tj, A. K. Jha, B. K. Ojha, S. Kumar, R. Kumar, *J. Phytopharm.* **2023**, *12*, 44.
- [18] X. Yan, M. Qi, P. Li, Y. Zhan, H. Shao, *Cell Biosci.* **2017**, *7*, 1.
- [19] D. Wróbel-Biedrawa, K. Grabowska, A. Galanty, D. Sobolewska, I. Podolak, *Life* **2022**, *12*, 591.
- [20] M. Wang, J. Firman, L. Liu, K. Yam, *BioMed Res. Int.* **2019**, *2019*, 7010467.
- [21] Y. Xu, X. Li, H. Wang, *Front. Nutr.* **2022**, *9*, 875826.
- [22] A. N. Panche, A. D. Diwan, S. R. Chandra, *J. Nutr. Sci.* **2016**, *5*, e47.
- [23] L. Ciomărnean, M. V. Milaciu, O. Runcan, S. C. Vesa, A. L. Răchișan, V. Negrean, M.-G. Perné, V. I. Donca, T.-G. Alexescu, I. Para, G. Dogaru, *Molecules* **2020**, *25*, 4320.
- [24] U. J. Jung, Y.-Y. Cho, M.-S. Choi, *Nutrients* **2016**, *8*, 305.
- [25] M. El-Badry, N. Haq, G. Fetih, F. Shakeel, *J. Chem. Eng. Data* **2014**, *59*, 839.
- [26] F. Shakeel, S. Alshehri, M. A. Ibrahim, E. M. Elzayat, M. A. Altamimi, K. Mohsin, F. K. Alanazi, I. A. Alsarra, *J. Mol. Liq.* **2017**, *234*, 73.
- [27] A. Golonko, A. J. Olichwier, A. Szklaruk, A. Paszko, R. Świsłocka, Ł. Szczerbiński, W. Lewandowski, *Molecules* **2024**, *29*, 2603.
- [28] M. Kazi, A. Alhajri, S. M. Alshehri, E. M. Elzayat, O. T. Meanazel, F. Shakeel, O. Noman, M. A. Altamimi, F. K. Alanazi, *Pharmaceutics* **2020**, *12*, 749.
- [29] I. Kazmi, F. A. Al-Abbasi, S. S. Imam, M. Afzal, M. S. Nadeem, H. N. Altayb, S. Alshehri, *Pharmaceutics* **2022**, *14*, 783.
- [30] A. M. Muqtader, F. Fatima, K. Anw, M. F. Aldawsa, G. A. Soliman, M. H. Fayed, *Int. J. Pharmacol.* **2020**, *16*, 460.
- [31] M. M. Ahmed, F. Fatima, M. A. Kalam, A. Alshamsan, G. A. Soliman, A. A. Shaikh, S. M. Alshahrani, M. F. Aldawsari, S. Bhatia, K. Anwer, *Saudi Pharm. J.* **2020**, *28*, 1817.
- [32] S. J. Gilani, M. N. Bin-Jumah, F. A. Al-Abbasi, M. S. Nadeem, S. S. Imam, S. Alshehri, M. M. Ahmed, M. M. Ghoneim, M. Afzal, S. I. Alzarea, *ACS Omega* **2022**, *7*, 23245.
- [33] P. Tran, Y.-C. Pyo, D.-H. Kim, S.-E. Lee, J.-K. Kim, J.-S. Park, *Pharmaceutics* **2019**, *11*, 132.
- [34] A. Vilatte, X. Spencer-Milnes, H. O. Jackson, S. Purton, B. Parker, *Microorganisms* **2023**, *11*, 512.
- [35] Y. Li, A. K. P. Mann, D. Zhang, Z. Yang, *Pharmaceutics* **2021**, *13*, 1307.
- [36] M. F. Aldawsari, K. Anwer, M. M. Ahmed, F. Fatima, G. A. Soliman, S. Bhatia, A. Zafar, M. A. Aboudzadeh, *Polymer* **2021**, *13*, 3512.
- [37] M. M. Ahmed, K. Anwer, G. A. Soliman, M. F. Aldawsari, A. A. Mohammed, S. Alshehri, M. M. Ghoneim, A. S. Alali, A. Alshetaili, A. Alalaiwe, *PeerJ* **2022**, *10*, e13482.
- [38] K. Anwer, M. M. Ahmed, M. F. Aldawsari, M. Iqbal, V. Kumar, *Pharmaceutics* **2022**, *16*, 19.
- [39] A. A. Alqahtani, M. M. Ahmed, A. A. Mohammed, J. Ahmad, *Pharmaceutics* **2023**, *15*, 1152.
- [40] S. Wang, X. Chen, X. Han, X. Hong, X. Li, H. Zhang, M. Li, Z. Wang, A. Zheng, *Pharmaceutics* **2023**, *15*, 416.

- [41] European Pharmacopoeia, *European Directorate for the Quality of Medicines & HealthCare*, 10th ed., Strasbourg, France **2019**.
- [42] M. K. Anwer, M. M. Ahmed, M. F. Aldawsari, S. Alshahrani, F. Fatima, M. N. Ansari, N. U. Rehman, R. I. Al-Shdefat, *Pharmaceuticals* **2020**, *13*, 255.
- [43] L. E. Vallejo, J. M. Espitia, B. Caicedo, *EPJ Web Conf.* **2017**, *140*, 3032.
- [44] G. Hao, Y. Hu, L. Shi, J. Chen, A. Cui, W. Weng, K. Osako, *Sci. Rep.* **2021**, *11*, 1646.
- [45] F. J. Osonga, A. Akgul, R. M. Miller, G. B. Eshun, I. Yazgan, A. Akgul, O. A. Sadiq, *ACS Omega* **2019**, *4*, 12865.
- [46] S. B. Schreiber, J. J. Bozell, D. G. Hayes, S. Zivanovic, *Food Hydrocolloids* **2013**, *33*, 207.
- [47] A. Zafar, N. K. Alruwaili, S. S. Imam, O. A. Alsaidan, M. M. Ahmed, M. Yasir, M. H. Warsi, A. Alquraini, M. M. Ghoneim, S. Alshehri, *Sensors* **2022**, *22*, 1364.
- [48] S. Zhu, S. Khalafi, Z. Chen, J. Poveda, D. Peng, H. Lu, M. Soutto, J. Que, M. Garcia-Buitrago, A. Zaika, W. Rifai, *Cancer Lett.* **2020**, *491*, 87.
- [49] T. Školáková, M. Slámová, A. Školáková, A. Kadeřábková, J. Patera, P. Zámotný, *Pharmaceuticals* **2019**, *11*, 383.
- [50] C. Godugu, A. R. Patel, R. Doddapaneni, J. Somagoni, M. Singh, *PLoS One* **2014**, *9*, e89919.
- [51] A. Ribeiro, A. Figueiras, D. Santos, F. Veiga, *AAPS PharmSci-Tech* **2008**, *9*, 1102.
- [52] D. R. Telange, A. T. Patil, A. M. Pethe, H. Fegade, S. Anand, V. S. Dave, *Eur. J. Pharm. Sci.* **2017**, *108*, 36.
- [53] M. M. Ahmed, F. Fatima, K. Anwer, M. F. Aldawsari, Y. S. M. Alsaidan, S. A. Alfaiz, A. Haque, A. Az, K. Alhazzani, *Chem. Phys. Lipids* **2020**, *233*, 105003.
- [54] M. K. Anwer, E. A. Ali, M. Iqbal, M. M. Ahmed, M. F. Aldawsari, A. A. Saqr, M. N. Ansari, M. A. Aboudzadeh, *Molecules* **2021**, *27*, 168.
- [55] E. H. Moglad, F. Fatima, M. M. Ahmed, V. D. Seshadri, K. Anw, M. F. Aldawsari, *Int. J. Pharmacol.* **2020**, *16*, 298.
- [56] F. Fatima, M. F. Aldawsari, M. M. Ahmed, K. Anwer, M. Naz, M. J. Ansari, A. M. Hamad, A. Zafar, M. Jafar, *Pharmaceuticals* **2021**, *13*, 1754.
- [57] M. M. Ahmed, F. Fatima, A. B. Mohammed, *J. Pharm. Res. Int.* **2020**, *32*, 29.
- [58] K. Anwer, M. M. Ahmed, A. Alshetaili, B. K. Almutairy, A. Alalaiwe, F. Fatima, M. N. Ansari, M. Iqbal, *J. Drug Deliv. Sci. Technol.* **2020**, *60*, 102101.
- [59] A. S. Alshetaili, R. Ali, W. Qamar, S. Almohizea, M. K. Anwer, *Int. J. Biol. Macromol.* **2023**, *246*, 125679.
- [60] M. M. Ahmed, K. Anwer, F. Fatima, M. F. Aldawsari, A. Alalaiwe, A. S. Alali, A. I. Alharthi, M. A. Kalam, *Polymer* **2022**, *14*, 2459.
- [61] M. A. Azad, D. Olawuni, G. Kimbell, A. Z. M. Badruddoza, S. Hossain, T. Sultana, *Pharmaceuticals* **2020**, *12*, 124.
- [62] M. P. Schwicker, N. D. Nikolov, M. Häßel, *Int. J. Mech. Eng. Robot. Res.* **2022**, *11*, 527.
- [63] M. M. Ahmed, F. Fatima, A. Alnami, M. Alsenaidy, A. H. Aodah, M. F. Aldawsari, B. Almutairy, K. Anwer, M. Jafar, *Polymer* **1825**, 2023, 15.

How to cite this article: A. S. Alali, M. Muqtader Ahmed, F. Fatima, Md. K. Anwer, M. Ibnauf, M. A. Aboudzadeh, *J. Appl. Polym. Sci.* **2024**, e56310. <https://doi.org/10.1002/app.56310>